

Sparsity Averaging for Compressive Imaging

Rafael E. Carrillo, Jason D. McEwen, Dimitri Van De Ville, Jean-Philippe Thiran, and Yves Wiaux

Abstract—We propose a novel regularization method for sparse image reconstruction from compressive measurements. The approach relies on the conjecture that natural images exhibit strong average sparsity over multiple coherent frames. The associated reconstruction algorithm, based on an analysis prior and a reweighted ℓ_1 scheme, is dubbed Sparsity Averaging Reweighted Analysis (SARA). We test our prior and the associated algorithm through extensive numerical simulations for spread spectrum and Gaussian acquisition schemes suggested by the recent theory of compressed sensing with coherent and redundant dictionaries. Our results show that average sparsity outperforms state-of-the-art priors that promote sparsity in a single orthonormal basis or redundant frame, or that promote gradient sparsity. We also illustrate the performance of SARA in the context of Fourier imaging, for particular applications in astronomy and medicine.

Index Terms—Compressed sensing, sparse approximation, image reconstruction, wavelet representation.

I. INTRODUCTION

The now famous theory of compressed sensing (CS) introduces a signal acquisition framework that goes beyond the traditional Nyquist sampling paradigm [1]–[4]. The fundamental premise in CS is that certain classes of signals, such as natural images, have a concise representation in terms of a sparsity basis where most of the coefficients are zero or small, and only few are significant. In the CS framework, a signal is sampled taking a few linear projections (measurements) onto a set of vectors and subsequently recovered using an optimization formulation that determines the sparsest representation consistent with the measurements [4]. Compressed sensing acquisition of data has an important impact on the design of imaging devices where data acquisition is expensive. A single pixel camera that acquires random projections from the visual scene through a digital micromirror array is detailed in [5]. Compressive hyper-spectral and optical imagers based on coded aperture are also proposed in the literature [6]. Compressive imaging strategies have also been proposed in medicine [7]–[9] and astronomy [10]–[12].

R. E. Carrillo is supported by the Swiss National Science Foundation (SNSF) under grant 200021-130359. J.D. McEwen is supported by a Newton International Fellowship from the Royal Society and the British Academy and, during this work, was also supported by a Leverhulme Early Career Fellowship from the Leverhulme Trust. Y. Wiaux is supported in part by the Center for Biomedical Imaging (CIBM) of the Geneva and Lausanne Universities, EPFL and the Leenaards and Louis-Jeantet foundations, and in part by the SNSF under grant PP00P2-123438.

R. E. Carrillo, D. Van De Ville, J.-P. Thiran and Y. Wiaux are with the Institute of Electrical Engineering, Ecole Polytechnique Fédérale de Lausanne (EPFL), CH-1015 Lausanne, Switzerland. D. Van De Ville and Y. Wiaux are also with the Department of Radiology and Medical Informatics, University of Geneva (UniGE), CH-1211 Geneva, Switzerland. J.D. McEwen is with the Department of Physics and Astronomy, University College London, London WC1E 6BT, U.K.

E-mail: rafael.carrillo@epfl.ch (R. E. Carrillo).

Sparse image representation assumes the ability to describe signals as linear combinations of a few atoms from a pre-defined dictionary. As such, the choice of the dictionary that sparsifies the signals is crucial for the success of this model. Orthonormal bases, especially wavelet bases, have been very popular in imaging linear inverse problems (see [13], [14] and references therein). However, there are numerous practical examples in which the signal of interest is not sparse in an orthonormal basis but rather in terms of an overcomplete dictionary. Thus the use of overcomplete dictionaries is now widespread in sparse signal and image processing [15]–[19]. Other approaches do not fix a pre-defined dictionary but instead learn the dictionary to perform best on a training set [20], [21].

The standard theory of CS tackles the case of signals sparse in the coordinate basis or in some other orthonormal basis, but recent works have begun to address the case of redundant dictionaries. Rauhut et al. find conditions on the dictionary such that the signal can be accurately recovered [22]. Candès et al. extend the CS theory to coherent and redundant dictionaries, providing theoretical stability guarantees based on general conditions of the sensing matrix, coined the Dictionary Restricted Isometry Property (D-RIP) [23]. The D-RIP is a natural extension of the standard RIP in CS [24]. In fact many random matrices that obey the standard RIP also obey the D-RIP, like Gaussian or Bernoulli ensembles. Also, the subsampled Fourier matrix multiplied by a random sign matrix satisfies the D-RIP [25], which falls within the framework of the recently proposed spread spectrum technique [26]. The theory promotes the use of analysis-based priors for signal recovery. CS with dictionary learning has also been studied. A best basis extension of CS, where an iterative thresholding algorithm performs both the recovery of the signal and the estimation of the best basis, is proposed in [27].

The reweighted ℓ_1 minimization scheme was proposed in [28] to approximate the ℓ_0 minimization behaviour. The algorithm replaces the ℓ_1 norm by a weighted ℓ_1 norm and solves a sequence of weighted ℓ_1 problems with weights essentially the inverse of the values of the solution of the previous problem. Empirical results have shown that this approach is very effective in reducing the number of measurements needed for accurate recovery compared to standard ℓ_1 minimization [23], [28], [29].

In the present work, we propose a novel sparsity analysis prior for compressive imaging in the context of the CS theory with coherent and redundant dictionaries. Our approach relies on the conjecture that natural images are simultaneously sparse in various frames, in particular wavelet frames, or in their gradient, so that promoting average signal sparsity over multiple frames is an extremely powerful prior. The associated reconstruction algorithm, based on an analysis prior

and a reweighted ℓ_1 scheme, is dubbed Sparsity Averaging Reweighted Analysis (SARA). We test SARA through extensive numerical simulations for spread spectrum and Gaussian acquisition schemes. Our results show that the average sparsity prior outperforms state-of-the-art priors that promote sparsity in a single orthonormal basis or redundant frame, or that promote gradient sparsity. We also depart from the theory and illustrate the performance of our conjecture and associated algorithm in the context of Fourier imaging, for particular applications in astronomy and medicine.

The organization of the remainder of the paper is as follows. In Section II, we review the theory of CS for both standard orthonormal bases and redundant dictionaries. Section III presents the SARA algorithm and practical considerations for its implementation. Numerical studies comparing SARA to state-of-the-art sparse reconstruction approaches are presented in Section IV. Finally we conclude in Section V with a discussion of our results, along with future work.

II. COMPRESSED SENSING

In this section, we recall the basics of compressed sensing. Firstly, we briefly review the standard compressed sensing theory for orthonormal bases. Secondly, we discuss recent results in compressed sensing with redundant dictionaries. Finally, we review the reweighted ℓ_1 minimization method for sparse signal recovery.

A. Compressed sensing with orthonormal bases

Consider a complex-valued signal $\mathbf{x} \in \mathbb{C}^N$ and also consider an orthonormal basis $\Psi \in \mathbb{C}^{N \times N}$, such that $\mathbf{x} = \Psi\boldsymbol{\alpha}$, $\boldsymbol{\alpha} \in \mathbb{C}^N$. The signal is said to be sparse if it contains only K non-zero coefficients in its decomposition, where $K \ll N$, or compressible if its ordered set of coefficients decays rapidly and the signal can be well approximated by just the first K coefficients.

CS demonstrates that a signal that is sparse, or compressible, in some basis can be acquired using a low-rate acquisition process that projects the signal onto a small set of vectors [1]–[4]. The signal \mathbf{x} is measured through the following model

$$\mathbf{y} = \Phi\mathbf{x} + \mathbf{n}, \quad (1)$$

where $\mathbf{y} \in \mathbb{C}^M$ denotes the measurement vector, $\Phi \in \mathbb{C}^{M \times N}$, $M < N$, is the sensing matrix and $\mathbf{n} \in \mathbb{C}^M$ represents the observation noise. The most common approach to recover \mathbf{x} from \mathbf{y} is to solve the so-called Basis Pursuit denoise problem [1], [2]:

$$\min_{\tilde{\boldsymbol{\alpha}} \in \mathbb{C}^N} \|\tilde{\boldsymbol{\alpha}}\|_1 \text{ subject to } \|\mathbf{y} - \Phi\Psi\tilde{\boldsymbol{\alpha}}\|_2 \leq \epsilon, \quad (2)$$

where ϵ is an upper bound on the ℓ_2 norm of the noise. Recall that the ℓ_p norm of a complex-valued vector $\mathbf{a} \in \mathbb{C}^M$ is defined as $\|\mathbf{a}\|_p \equiv (\sum_{i=1}^M |a_i|^p)^{1/p}$, where $|\cdot|$ represents the modulus of a complex number. The signal is recovered as $\hat{\mathbf{x}} = \Psi\hat{\boldsymbol{\alpha}}$, where $\hat{\boldsymbol{\alpha}}$ denotes the solution to (2). Such problems solving for the representation of the signal in a sparsity basis are known as synthesis-based problems. The theory shows that the Basis Pursuit denoise problem can recover \mathbf{x} if the sensing

matrix obeys certain properties like the Restricted Isometry Property (RIP) [24] or the mutual coherence [30]. A family of iterative greedy algorithms are also proposed in the literature that offer similar recovery guarantees [31]–[33].

B. Compressed sensing with coherent and redundant dictionaries

The techniques presented in the previous subsection hold for signals that are sparse in the standard coordinate basis or sparse with respect to some other orthonormal basis. However, there are numerous practical examples in which a signal of interest is not sparse in a single orthonormal basis but over several orthonormal bases or over an overcomplete dictionary [16], [18], [19]. In this setting the signal \mathbf{x} is now expressed in terms of a dictionary $\Psi \in \mathbb{C}^{N \times D}$, $N < D$, as $\mathbf{x} = \Psi\boldsymbol{\alpha}$, $\boldsymbol{\alpha} \in \mathbb{C}^D$. Since $M \ll N < D$, the problem is more severely underdetermined when solving for the signal in the sparsity basis. Rauhut et al. found in [22] that incoherence in the dictionary Ψ is needed such that the compound matrix $\Phi\Psi$ obeys the RIP to accurately recover $\boldsymbol{\alpha}$. Recall that the coherence of two dictionaries (or one dictionary with itself) may be defined as the maximum absolute value of the scalar product between their atoms [30].

As opposed to synthesis-based problems, which find the sparse representation vector $\boldsymbol{\alpha}$, analysis-based problems recover the signal itself by solving the following problem [34]:

$$\min_{\tilde{\mathbf{x}} \in \mathbb{C}^N} \|\Psi^\dagger \tilde{\mathbf{x}}\|_1 \text{ subject to } \|\mathbf{y} - \Phi\tilde{\mathbf{x}}\|_2 \leq \epsilon, \quad (3)$$

where \dagger denotes the conjugate transpose operation. In the case of orthonormal bases Ψ the two approaches are equivalent. However, when Ψ is a frame or an overcomplete dictionary, the two problems are no longer equivalent. The geometry of the two problems are studied by Elad et al. in [34], who show that there is a large gap between the two formulations due to substantial difference in their geometrical structures. Note that the analysis problem does not increase the dimensionality of the problem when overcomplete dictionaries are used. Empirical studies have shown very promising results for the analysis approach [34]. Theoretical properties of the ℓ_1 analysis regularization for inverse problems and its robustness against noise are studied in [35].

Candès et al. provide a theoretical analysis of the ℓ_1 analysis problem coupled with redundant dictionaries in [23]. They extend the compressed sensing theory to coherent and redundant dictionaries, as opposed to the synthesis results in [22], providing theoretical stability guarantees based on a generalization of the RIP of the sensing matrix Φ , the so-called D-RIP. These results have been proven for the case of real-valued signals only. In the following we define the D-RIP. Let Ψ be an overcomplete dictionary. Also, let Σ_K be the union of all subspaces spanned by all subsets of K columns of Ψ . The measurement matrix Φ obeys the D-RIP with constant $\delta_K \in (0, 1)$ if

$$(1 - \delta_K)\|\mathbf{v}\|_2^2 \leq \|\Phi\mathbf{v}\|_2^2 \leq (1 + \delta_K)\|\mathbf{v}\|_2^2 \quad (4)$$

holds for all $\mathbf{v} \in \Sigma_K$.

The D-RIP is a natural extension of the standard RIP. In fact many random matrices that obey the standard RIP also obey the D-RIP, like Gaussian or Bernoulli ensembles, provided that $M = O(K \log(D/K))$. Also, a result by Krahmer and Ward implies that the subsampled Fourier matrix multiplied by a random sign matrix satisfies the D-RIP, which provides a fast sensing operator [25]. Interestingly, this approach falls within the framework of the recently proposed spread spectrum technique [26]. If Φ satisfies the D-RIP with $\delta_K < 0.08$ and Ψ is a general frame, Candès et al. prove in [23] that the solution to (3) \hat{x} satisfies the following error bound:

$$\|\hat{x} - x\|_2 \leq C_0 \epsilon + C_1 \frac{\|\Psi^\dagger x - (\Psi^\dagger x)_K\|_1}{\sqrt{K}}, \quad (5)$$

where $(\Psi^\dagger x)_K$ denotes the best K -term approximation of $\Psi^\dagger x$ and C_0 and C_1 are numerical constants.

C. Reweighted ℓ_1 minimization

The reweighted ℓ_1 minimization algorithm was proposed by Candès et al. in [28] to simulate the ℓ_0 minimization behaviour. The algorithm replaces the ℓ_1 norm by a weighted ℓ_1 norm $\|Wx\|_1$, where W is a diagonal matrix with positive weights. The algorithm solves a sequence of weighted ℓ_1 problems with weights essentially the inverse of the values of the solution of the previous problem. The idea behind this formulation is that large weights will encourage small entries in the solution vector, and small weights will encourage larger values in the corresponding entries. This scheme has been observed to be very effective in reducing the number of measurements needed for recovery, and to outperform standard ℓ_1 minimization in many situations, see e.g. [23], [28], [29].

III. SPARSITY AVERAGING REWEIGHTED ANALYSIS

In this section we propose a novel algorithm for compressive imaging problems based on the prior of average signal sparsity over multiple coherent frames. We start by discussing our conjecture of average signal sparsity. Then, we propose the reweighted ℓ_1 analysis method as a means to promote average sparsity and present the resulting algorithm. Finally, we detail the optimization methods used to solve the reweighted ℓ_1 problem in the proposed algorithm.

A. Average sparsity conjecture and associated analysis prior

Natural images are often complicated and several types of structures can be present at once. It is well known that piecewise smooth images exhibit gradient sparsity, and that images with extended structures are better encapsulated in wavelet frames. Therefore, we here conjecture that promoting average sparsity or compressibility over multiple frames rather than single frames is an extremely powerful prior.

We propose using a dictionary composed of a concatenation of q frames, i.e.

$$\Psi = \frac{1}{\sqrt{q}}[\Psi_1, \Psi_2, \dots, \Psi_q], \quad (6)$$

with $\Psi \in \mathbb{C}^{N \times D}$, $N < D$. The analysis-based framework is a nice approach to promote average sparsity. The prior

$$\|\Psi^\dagger \bar{x}\|_1 \sim \frac{1}{q} \sum_{i=1}^q \|\Psi_i^\dagger \bar{x}\|_1 \quad (7)$$

can indeed be considered, which is a convex relaxation of average sparsity

$$\|\Psi^\dagger \bar{x}\|_0 \sim \frac{1}{q} \sum_{i=1}^q \|\Psi_i^\dagger \bar{x}\|_0. \quad (8)$$

Note that in this setting each frame contains all the signal information. Such a prior cannot be formulated in a synthesis-based perspective. Previous works considering multiple frames, e.g. [15]–[17], consider a component separation approach, decomposing the signal as $x = \sum_{i=1}^q x_i$, where each component x_i is sparse in the i -th frame. This is a completely different problem, where each component bears only part of the signal information, which can be address either in an analysis or in a synthesis framework.

Note on a theoretical level that a single signal cannot be arbitrarily sparse simultaneously in any pair of incoherent frames. For example, a signal extremely sparse in the Dirac basis is completely spread in the Fourier basis and thus (5) does not provide a good error bound. As discussed by Candès et al. in [23], what is important is that the columns of the Gram matrix $\Psi^\dagger \Psi$ are reasonably sparse such that $\Psi^\dagger x$ is sparse when x admits a sparse representation α such that $x = \Psi \alpha$. This requirement is nothing else than a coherence condition on Ψ . In our case of concatenations of frames, this leads to the condition that each Ψ_i is highly coherent with itself and with the other frames.

The concatenation of the first eight orthonormal Daubechies wavelet bases (Db1-Db8, $q = 8$) represents a natural choice in this context. The first Daubechies wavelet basis, Db1, is the Haar wavelet basis and, in particular, it can be used as an alternative to gradient sparsity (usually imposed by a total variation prior [36], [37]) to promote piecewise smooth signals. The Db2-Db8 bases are coherent with Haar, in particular due to their compact support and identical sampling positions, while providing smoother decompositions. Also note that the approaches in [15]–[17] use incoherent frames for the decomposition, while our average sparsity prior takes the opposite direction.

B. Constrained reweighted ℓ_1 analysis problem

For what concerns the approach to combine the prior and the data, we choose to solve a constrained problem, minimizing the priori functional subject the a bound on the residual noise power. Such problems offer a strong fidelity term when the noise power is known, so that a precise value can be estimated for the bound on the residual noise. On the contrary, unconstrained minimization problems, using a weighted sum of the prior and of the residual noise power would resort to an arbitrary weight parameter that can not be evaluated from the noise power. These considerations naturally lead us to the same minimization problems as those promoted in the context of CS with redundant dictionaries, to which we add a

reweighting scheme promoting ℓ_0 . The weighted ℓ_1 analysis problem is defined as

$$\min_{\mathbf{x} \in \mathbb{C}^N} \|\mathbf{W}\Psi^\dagger \hat{\mathbf{x}}\|_1 \text{ subject to } \|\mathbf{y} - \Phi \hat{\mathbf{x}}\|_2 \leq \epsilon, \quad (9)$$

where $\mathbf{W} \in \mathbb{R}^{D \times D}$ is a diagonal matrix with positive weights. Assuming i.i.d. complex Gaussian noise with variance σ_n , the ℓ_2 norm term in (9) is identical to a bound on the χ^2 distribution with $2M$ degrees of freedom governing the noise level estimator. Therefore, we set this bound as $\epsilon^2 = (2M + 4\sqrt{M})\sigma_n^2/2$, where $\sigma_n^2/2$ is the variance of both the real and imaginary parts of the noise. This choice provides a likely bound for $\|\mathbf{n}\|_2$, since the probability that $\|\mathbf{n}\|_2^2$ exceeds ϵ^2 is the probability that a χ^2 with $2M$ degrees of freedom exceeds its mean, $2M$, by at least two times the standard deviation $2\sqrt{M}$, which is very small. The solution to (9) is denoted as $\Delta(\mathbf{y}, \Phi, \mathbf{W}, \epsilon)$, which is a function of the data vector \mathbf{y} , the measurement and weight matrices Φ and \mathbf{W} respectively, and the bound ϵ on the noise level estimator.

In the reweighting approach a sequence of weighted ℓ_1 problems is solved to approximate the behaviour of the ℓ_0 problem. As an illustration suppose that the sparse signal \mathbf{x} is known *a priori* and that we set the weights as $W_{ii} = |x_i|^{-1}$. In this case the weights are infinite at all locations where the signal is zero, forcing the coordinates of the solution vector at these locations to be zero. This set of weights makes the weighted norm independent of the precise value of the non-zero components and guarantees recovery of the correct solution assuming only $K < M$. In practice, the original signal is not known in advance but we can compute the appropriate weights by solving sequentially weighted ℓ_1 problems, each using as weights essentially the inverse of the values of the solution of the previous problem.

As it is not possible to have infinite weights where the estimated signal values are zero, a stability parameter must also be added to the signal value in the selection of the weights. In practice, we update the weights at each iteration, i.e. after solving a complete weighted ℓ_1 problem, by the function

$$f(\gamma, a) \equiv \frac{\gamma}{\gamma + |a|}, \quad (10)$$

where γ plays the role of a stabilization parameter (ideally zero), avoiding undefined weights when the signal value is zero. Note that as $\gamma \rightarrow 0$ the weighted ℓ_1 norm approaches the ℓ_0 norm. To approximate the ℓ_0 norm by the reweighted ℓ_1 algorithm, we use a homotopy strategy [38] and solve a sequence of weighted ℓ_1 problems using a decreasing sequence $\{\gamma^{(t)}\}$, with t denoting the iteration time variable. Under this scheme, a weighted ℓ_1 problem is first solved and its solution is used as the warm start initialization for the next problem that is geometrically closer to the ℓ_0 problem. This process is then repeated until the solution becomes stationary [38].

C. The SARA algorithm

The resulting algorithm after the previous considerations, dubbed sparsity averaging reweighted analysis (SARA), is defined in Algorithm 1. Note that in [12] some of the

authors have presented the application of SARA to radio-interferometric imaging in astronomy. A rate parameter β , with $0 < \beta < 1$, controls the decrease of the sequence $\gamma^{(t)} = \beta\gamma^{(t-1)} = \beta^t\gamma_0$ such that $\gamma^{(t)} \rightarrow 0$ as $t \rightarrow \infty$. Ideally, $\gamma^{(t)}$ should decrease to zero, but since we have noise, we set a lower bound as $\gamma^{(t)} \geq \sigma_\alpha$. The standard deviation of the noise in the representation domain is computed as $\sigma_\alpha = \sqrt{M/qN}\sigma_n$, which gives a rough estimate for a baseline above which significant signal components could be identified. As a starting point we set $\hat{\mathbf{x}}^{(0)}$ as the solution of the ℓ_1 problem and $\gamma^{(0)} = \sigma_s(\Psi^T \hat{\mathbf{x}}^{(0)})$, where $\sigma_s(\cdot)$ stands for the empirical standard deviation of the signal, to fix the signal scale. The reweighting process ideally stops when the relative variation between successive solutions $\|\hat{\mathbf{x}}^{(t)} - \hat{\mathbf{x}}^{(t-1)}\|_2 / \|\hat{\mathbf{x}}^{(t-1)}\|_2$ is smaller than some bound η , with $0 < \eta < 1$, or after the maximum number of iterations allowed, N_{\max} , is reached. In our implementation, which will be detailed in Section III-D, we fix $\eta = 10^{-3}$ and $\beta = 10^{-1}$.

Algorithm 1 SARA algorithm

Input: $\mathbf{y}, \Phi, \epsilon, \sigma_\alpha, \beta, \eta$ and N_{\max} .

Output: Reconstructed image $\hat{\mathbf{x}}$.

- 1: Initialize $t = 1$, $\mathbf{W}^{(0)} = \mathbf{I}$ and $\rho = 1$.
 - 2: Compute

$$\hat{\mathbf{x}}^{(0)} = \Delta(\mathbf{y}, \Phi, \mathbf{W}^{(0)}, \epsilon),$$

$$\gamma^{(0)} = \sigma_s(\Psi^\dagger \hat{\mathbf{x}}^{(0)}).$$
 - 3: **while** $\rho > \eta$ and $t < N_{\max}$ **do**
 - 4: Update the weight matrix

$$\mathbf{W}_{ij}^{(t)} = f(\gamma^{(t-1)}, \hat{\alpha}_i^{(t-1)}) \delta_{ij}, \text{ for } i, j = 1, \dots, D$$
 with $\hat{\alpha}^{(t-1)} = \Psi^T \hat{\mathbf{x}}^{(t-1)}$
 - 5: Compute a solution

$$\hat{\mathbf{x}}^{(t)} = \Delta(\mathbf{y}, \Phi, \mathbf{W}^{(t)}, \epsilon).$$
 - 6: Update $\gamma^{(t)} = \max(\beta\gamma^{(t-1)}, \sigma_\alpha)$.
 - 7: Update $\rho = \|\hat{\mathbf{x}}^{(t)} - \hat{\mathbf{x}}^{(t-1)}\|_2 / \|\hat{\mathbf{x}}^{(t-1)}\|_2$
 - 8: $t \leftarrow t + 1$
 - 9: **end while**
 - 10: **return** $\hat{\mathbf{x}}$
-

D. Solving the weighted ℓ_1 problem

The SARA algorithm needs to solve (9) at each iteration. This convex problem involves the minimization of a non-differentiable function, which rules out smooth optimization techniques. To solve (9), we use the Douglas-Rachford splitting algorithm, tailored to solve problems of the form

$$\min_{\mathbf{x} \in \mathbb{R}^N} f_1(\mathbf{x}) + f_2(\mathbf{x}), \quad (11)$$

where $f_1(\mathbf{x})$ and $f_2(\mathbf{x})$ are convex lower semicontinuous functions from \mathbb{R}^N to \mathbb{R} , with the important property of not requiring differentiability of any of the functions [39]. Note that any convex constrained problem can be formulated as an unconstrained problem by using the indicator function of the convex constraint set as one of the functions in (11), i.e. $f_k(\mathbf{x}) = i_C(\mathbf{x})$ where C represents the constraint set. Also note that complex-valued vectors are treated as real-valued vectors with twice the dimension (accounting for real and

imaginary parts). The Douglas-Rachford algorithm belongs to the family of proximal splitting methods. The key concept in these methods is the use of the proximity operator of a convex function, which is a natural extension of the notion of a projection operator onto a convex set. For example, the proximal operator of the ℓ_1 norm is the soft-thresholding operator, and the proximal operator of the indicator function of a constraint is simply the projection operator onto the constraint set. We give a formal definition of the proximity operator in Appendix A. Proximal splitting methods proceed by splitting the contribution of the functions f_1 and f_2 individually so as to yield an easily implementable algorithm. They are called proximal because each non-smooth function in (11) is involved in the minimization via its proximity operator. See [40] for a review of proximal splitting methods and their applications in signal and image processing.

The problem in (9) can be reformulated as in (11), with $f_1(\mathbf{x}) = \|\mathbf{W}\Psi^\dagger \mathbf{x}\|_1$ and $f_2(\mathbf{x}) = i_{C_\epsilon}(\mathbf{x})$, where $C_\epsilon = \{\mathbf{x} \in \mathbb{C}^N : \|\mathbf{y} - \Phi \mathbf{x}\|_2 \leq \epsilon\}$. Since many image processing applications deal with intensity images, one may want to add a reality and positivity constraint on the estimated signal. Then one can define $f_2(\mathbf{x}) = i_{C'_\epsilon}(\mathbf{x})$, where $C'_\epsilon = C_\epsilon \cup \mathbb{R}_+^N$. The general form of the Douglas-Rachford algorithm is presented in Algorithm 2. The sequence $\{\mathbf{x}^{(t)}\}$ generated by Algorithm 2 has been proved to converge to a solution of problem (11) [39]. The algorithm is stopped when the relative variation between the objective function evaluated at successive solutions, $|f_1(\mathbf{x}^{(t)}) - f_1(\mathbf{x}^{(t-1)})| / |f_1(\mathbf{x}^{(t-1)})|$, is smaller than some bound ξ , with $0 < \xi < 1$, or after the maximum number of iterations allowed, M_{\max} , is reached. $\nu > 0$ and $0 < \tau_t < 2$ are convergence parameters. In our implementation we use the values $\tau_t = 1, \forall t, \xi = 10^{-3}$ and $\nu = 10^{-1}$. We detail the implementation of the proximity operators of f_1 and f_2 in Appendix A.

Algorithm 2 Douglas-Rachford algorithm

- 1: Initialize $t = 1, \mathbf{x}^{(1)} \in \mathbb{C}^N, \tau_t \in (0, 2), \xi \in (0, 1)$ and $\nu > 0$.
 - 2: **while** $\zeta > \xi$ and $t < M_{\max}$ **do**
 - 3: $\mathbf{z}^{(t)} = \text{prox}_{\nu f_2}(\mathbf{x}^{(t)})$.
 - 4: $\mathbf{x}^{(t+1)} = \mathbf{x}^{(t)} + \tau_t (\text{prox}_{\nu f_1}(2\mathbf{z}^{(t)} - \mathbf{x}^{(t)}) - \mathbf{z}^{(t)})$.
 - 5: $\zeta = |f_1(\mathbf{x}^{(t)}) - f_1(\mathbf{x}^{(t-1)})| / |f_1(\mathbf{x}^{(t-1)})|$.
 - 6: $t \leftarrow t + 1$
 - 7: **end while**
 - 8: **return** $\mathbf{x}^{(t)}$
-

IV. EXPERIMENTAL RESULTS

In this section we evaluate the performance of the SARA algorithm through numerical simulations. Firstly, we detail the experimental set-up, describing the practical implementation of SARA and algorithms used as benchmarks. Secondly, we report the results of the comparison of SARA to the benchmark methods. Finally, we illustrate the application of SARA for Fourier imaging in astronomy and medicine.

A. Experimental set-up

In light of our discussion in Section III-A, for all experiments we consider SARA as built from a concatenation of the first eight orthonormal Daubechies wavelet bases, Db1-Db8. We use a fourth order decomposition depth for all wavelet bases. This choice results from a test over variations on the number of bases and decomposition depths (see Section IV-B).

We compare SARA to analogous analysis algorithms, where the average sparsity prior is simply substituted for a state-of-the-art prior promoting sparsity in a single orthonormal basis or redundant frame, or in the gradient. These priors are implemented through the very same constrained analysis ℓ_1 and TV minimization problems (reweighted or not). The comparison is performed in terms of reconstruction quality and computation time. In practice, the non-reweighted ℓ_1 problems are defined through (3) with three different options for Ψ : the Daubechies 8 wavelet basis, the redundant curvelet frame [19] and the concatenation of the eight bases described above for SARA. The associated algorithms are respectively denoted BPDb8, Curvelet and BPSA. The reweighted ℓ_1 problems considered are defined through the reweighting procedure described in Section III-B based on (9), for each of the three frames considered: the Daubechies 8 wavelet basis, the curvelet frame, and the concatenation of Db1-Db8 leading to SARA. The associated algorithms are respectively denoted RW-BPDb8, RW-Curvelet and SARA. The TV minimization problem is formulated as a constrained problem like (3), but replacing the ℓ_1 norm by the image TV norm. The TV norm is defined by the ℓ_1 norm of the magnitude of the gradient of the signal $\|\bar{\mathbf{x}}\|_{\text{TV}} = \|\nabla \bar{\mathbf{x}}\|_1$, where $\nabla \bar{\mathbf{x}}$ denotes the gradient magnitude [36]. The reweighted version of TV, still through the procedure defined in Section III-B, is denoted as RW-TV. Since all the images of interest are positive, we impose the additional constraint that $\bar{\mathbf{x}} \in \mathbb{R}_+^N$ for all problems.

We use as reconstruction quality metric the signal to noise ratio (SNR), which is defined as:

$$\text{SNR} = 20 \log_{10} \left(\frac{\|\mathbf{x}\|_2}{\|\mathbf{x} - \hat{\mathbf{x}}\|_2} \right), \quad (12)$$

where \mathbf{x} and $\hat{\mathbf{x}}$ denote the the original image and the estimated image respectively. The measurements are corrupted by complex Gaussian noise in general with a fixed input SNR. The input SNR is defined as $\text{ISNR} = 20 \log_{10}(\|\mathbf{y}_0\|_2 / \|\mathbf{n}\|_2)$, where \mathbf{y}_0 identifies the clean measurement vector.

B. Simulations and results for spread spectrum and Gaussian measurements

In this subsection we evaluate the reconstruction performance of SARA by recovering well-known test images from compressive measurements following the model in (1). We use 256×256 pixel versions of Lena and cameraman as test images. In order to have a fast measurement operator that obeys the D-RIP, we use for a first experiment the spread spectrum technique described in [26]. Spread spectrum incorporates a modulating sequence in the measurement operator defining it as $\Phi = \text{MFC}$, where $\mathbf{C} \in \mathbb{R}^{N \times N}$ is a diagonal matrix with elements with unit norm and randomized sign, $\mathbf{F} \in \mathbb{C}^{N \times N}$

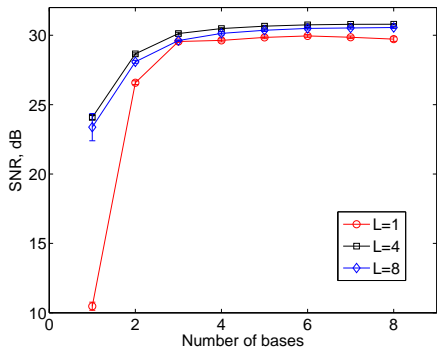


Figure 1. Reconstruction quality as a function of the number of bases in the dictionary for decomposition depths $L = 1, 4, 8$. Results for Lena with $M = 0.3N$ and ISNR set to 30 dB.

is the discrete Fourier operator and $M \in \mathbb{R}^{M \times N}$ is a binary mask defining the random selection operator.

Prior to our main analysis, we evaluate the reconstruction performance of SARA as a function of the number of wavelet bases in the dictionary. We test decomposition depths $L = 1, 4, 8$ for all dictionaries. We add bases in parametric order, i.e., one basis means Db1 alone, two bases Db1 and Db2 and so on until we reach the eight bases from Db1-Db8. The results for Lena are summarized in Figure 1. We can observe that the best performance is obtained when $L = 4$ and the worst when $L = 1$. We can also observe that the reconstruction quality improves as the number of bases increases until it saturates between 4 to 8 bases. This results corroborates our choice for 8 bases, and depth $L = 4$. Results for cameraman lead to the same conclusion.

Having validated the dictionary choice, we now proceed to evaluate the reconstruction quality of SARA as a function of the undersampling ratio M/N . We vary the undersampling ratio from 0.1 to 0.9. The SNR results comparing SARA against all the other benchmark methods are shown in Figures 2 (a) and 2 (d) for Lena and cameraman respectively. Average values over 30 simulations and associated one-standard-deviation error bars are reported. The results demonstrate that SARA outperforms state-of-the-art methods for all undersampling ratios. SARA achieves gains between 0.7 and 1.4 dB for cameraman and between 0.9 and 1.9 dB for Lena. The largest gains are observed for undersampling ratios in the range 0.2-0.5 for both images. Notably, BPSA achieves better SNRs than BPDdb8, curvelet and their reweighted versions for all undersampling ratios. It also achieves similar SNRs to TV for undersampling ratios in the range 0.4-0.9.

Computation times (in seconds) as a function of the undersampling ratio M/N are reported in Figures 2 (b) and 2 (e), for Lena and cameraman respectively. Times are measured on a 2.4 GHz Xeon quad core for MATLAB implementations of all the algorithms. Again, average values over 30 simulations and associated one-standard-deviation error bars are reported. Although the concatenation of multiple bases render the algorithm structure more costly, we see that the computation times are of the order of minutes for SARA, being very similar to those required for RW-BPDdb8 for undersampling ratios larger than 0.3. We can also observe that SARA is faster than RW-

TV and RW-Curvelet while achieving better reconstruction quality. Note also that BPSA is faster than TV.

The next experiment studies the robustness of SARA against noise in the measurements. We fix the number of measurements as $M = 0.2N$ and add Gaussian noise to the measurements varying the input noise with ISNR in the range 0 to 40 dB. The results are summarized in Figures 2 (c) and 2 (f) for Lena and cameraman respectively. Average values over 30 simulations and associated one-standard-deviation error bars are reported. As expected from the bound in (5), the relationship between SNR and ISNR is linear for low ISNRs until it is high enough and the reconstruction quality is dominated by the undersampling effect. Notably, SARA outperforms the benchmark methods in both test images for all ISNRs, achieving SNRs of 20 dB for ISNRs of 0 dB. Again, BPSA yields a better performance than BPDdb8, Curvelet and their reweighted versions.

Next we present a visual assessment of the reconstruction quality of SARA compared to the benchmark methods. Figure 3 shows the results from Lena and cameraman for $M = 0.2N$ and ISNR of 30 dB. The first row show the original images. We only show the best image for each prior: reweighted or non-reweighted. Thus the results are shown for SARA, RW-TV, BPDdb8 and Curvelet. SARA achieves, for cameraman and Lena respectively, a gain of 1.4 and 1.8 dB over RW-TV, which is the second best method. Moreover, beyond an SNR increase, SARA provides an impressive reduction of visual artifacts relative to the other methods in this high undersampling regime, as is evident from the reconstructions. In particular RW-TV exhibits expected cartoon-like artifacts. BPDdb8 and Curvelet do not yield results of comparable quality relative to SARA, neither in SNR nor visually.

As final experiment in this subsection, we study the performance of SARA with Gaussian random matrices as measurements operators. For this experiment we use a cropped version of Lena, around the head, of dimension 128×128 as test image (due to computational limitations for the use of a dense sensing matrix). We compare SARA against all the benchmark methods for this sensing modality. We evaluate the reconstruction quality as a function of the undersampling ratio M/N in the range 0.1 to 0.9. ISNR is set to 30 dB. The SNR results are reported in Figures 4. Average values over 30 simulations and associated one-standard-deviation error bars are reported. These results confirm the performance of SARA in compressive image reconstruction with a different sensing matrix. For $M = 0.1N$ SARA is 1 dB below TV and RW-TV and for $M = 0.2N$ SARA achieves an SNR almost identical to RW-TV and TV. For the rest of undersampling ratios SARA outperforms the benchmark methods, achieving a gain between 0.8 and 1.2 dB over RW-TV (second best method).

C. Fourier imaging illustrations

Here we illustrate potential applications of SARA in the context of Fourier imaging, specifically for aperture synthesis for radio-interferometric imaging in radio astronomy [41] and magnetic resonance imaging in medicine [42]. For both techniques, the measurement operator can be modeled as

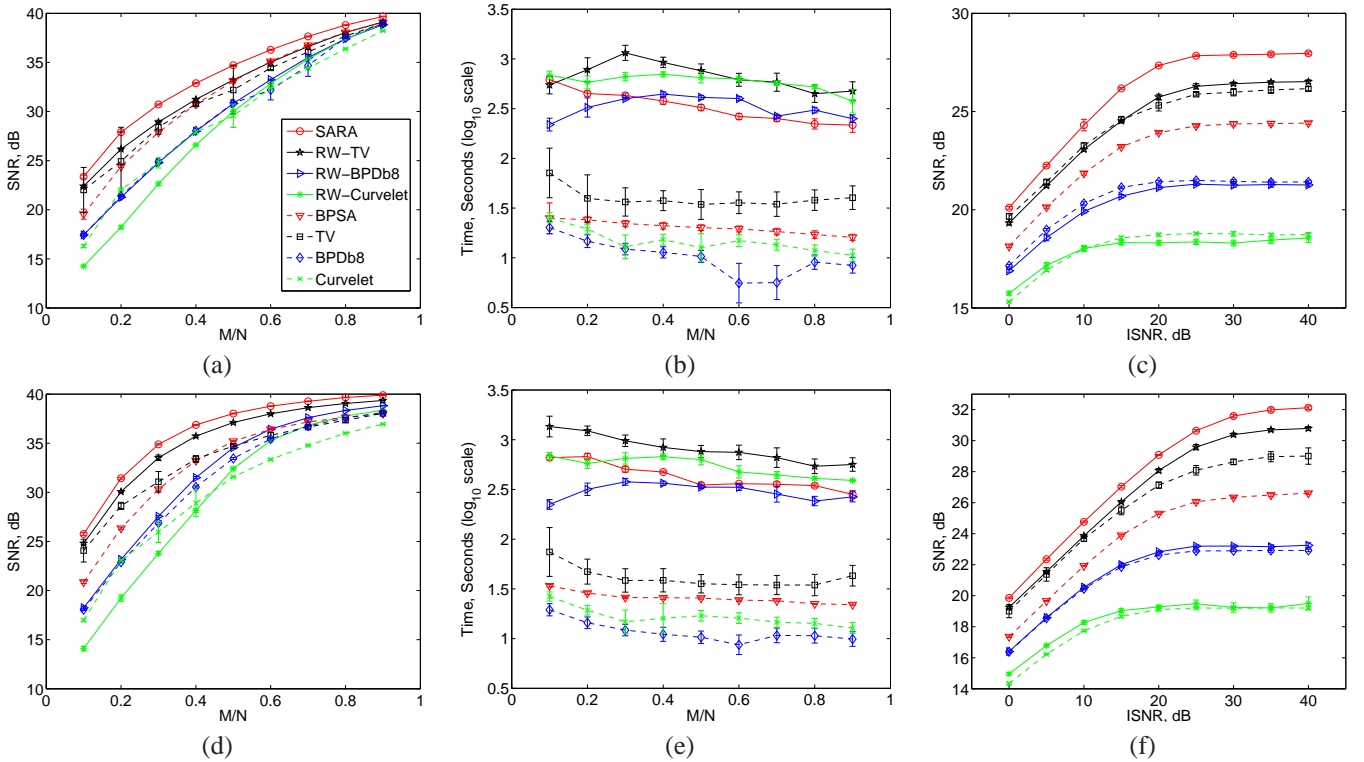


Figure 2. Reconstruction quality results for spread spectrum measurements. First column shows SNR results against the undersampling ratio for: (a) Lena and (d) cameraman. ISNR set to 30 dB. Second column shows the respective average computation times for: (b) Lena and (e) cameraman. Third column shows SNR as a function of ISNR for (c) Lena and (f) cameraman. Undersampling fixed to $M = 0.2N$.

$\Phi = MF$, where $F \in \mathbb{C}^{N \times N}$ is the discrete Fourier operator and $M \in \mathbb{R}^{M \times N}$ is a binary matrix representing the sampling profile. We consider measurements generated from random variable density sampling profiles. Such profiles allow one to account for the fact that most of the signal energy is usually concentrated around low frequencies, also mimicking common generic sampling patterns in these fields [8], [10], [12]. See [43] for the exact shape of the density profile. Since we consider intensity images, only a half Fourier plane is sampled.

For this experiment, we compare SARA to essentially the same benchmark methods. We however consider a concatenation of nine bases as the dictionary for SARA and BPSA. The first basis is the Dirac basis and the eight remaining bases are the first eight Daubechies wavelets, Db1-Db8. The reason to add the Dirac basis is that the images of interest are also sparse in the spatial domain. This does not break the overall coherence condition on Ψ because of the compact support of the Daubechies wavelets. Also for these illustrations we consider the redundant frame of isotropic undecimated wavelets [18], used previously in astronomy [44], instead of curvelets. The associated non-reweighted and reweighted methods are respectively denoted IUWT and RW-IUWT.

For the radio-interferometric imaging illustration we use a cropped version of the radio galaxy Cygnus A [45], of dimension 300×526 , as test image. We take a very adverse undersampling ratio $M = 0.05N$ and set ISNR to 30 dB. The first two rows of Figure 5 show the test image and the backprojected image, which is defined as $F^H M^T \mathbf{y}$. The SNR of the recovered image for each algorithm is as follows:

SARA (39.4 dB), BPSA (32.9 dB), RW-TV (24.6 dB), TV (28.6 dB), RW-BPD8 (35.9 dB), BPD8 (35.5 dB), RW-IUWT (25.5 dB) and IUWT (26.3 dB). SARA achieves the best SNR followed by RW-BPD8. The last two rows of Figure 5 show reconstructed images for SARA and RW-BPD8. In addition to an SNR gain of 3.5 dB, SARA achieves a reconstruction with less visual artifacts, though a loss of resolution must also be acknowledged in this extreme undersampling regime. A detailed study of the application of SARA to radio-interferometric imaging is presented in [12].

For the magnetic resonance imaging illustration we reconstruct a 224×168 brain image for the same adverse undersampling ratio $M = 0.05N$, which is unprecedented in the field. ISNR is set as 30 dB. The first row of Figure 6 show the original brain image and the backprojected image. The SNR of the recovered image for each algorithm is as follows: SARA (18.8 dB), BPSA (17.6 dB), RW-TV (16.9 dB), TV (17.3 dB), RW-BPD8 (15.6 dB), BPD8 (16.3 dB), RW-IUWT (16.2 dB) and IUWT (16.1 dB). SARA achieves the best SNR, followed by BPSA and TV. In the second row of Figure 6 we show reconstructed images for SARA and TV. In addition to an SNR gain of 1.5 dB, SARA achieves an impressively better reconstruction from the visual standpoint.

V. CONCLUSION AND DISCUSSION

In this paper we have proposed a novel regularization method for compressive image reconstruction along with its associated algorithm, dubbed Sparsity Averaging Reweighted Analysis (SARA). The approach relies on the conjecture that



Figure 3. Reconstruction example for Lena (left) and cameraman (right), $M = 0.2N$ and ISNR set as 30 dB. Top row: original images. Left column from top to bottom, reconstructed images for: SARA (28.1 dB), RW-TV (26.3 dB), BPDb8 (21.4 dB) and Curvelet (18.7 dB). Right column from top to bottom, reconstructed images for: SARA (31.5 dB), RW-TV (30.1 dB), BPDb8 (22.9 dB) and Curvelet (23.1 dB).

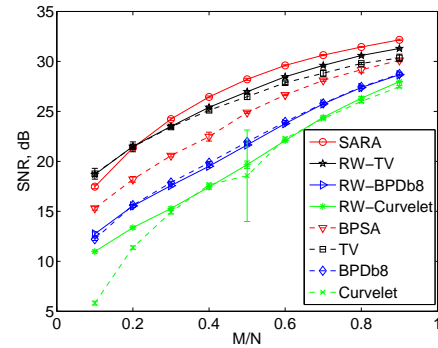


Figure 4. Reconstruction quality against the undersampling ratio for cropped Lena image. Random Gaussian matrix as sensing matrix. ISNR set to 30 dB.

natural images are simultaneously sparse in multiple frames, in particular wavelet frames, or in their gradient, so that promoting average signal sparsity over multiple coherent frames is an extremely powerful prior. The proposed constrained reweighted analysis algorithm is evaluated under three different measurement schemes: spread spectrum and random Gaussian measurements, that are within the theory of CS with coherent and redundant dictionaries, and Fourier imaging for illustrative applications in astronomy and medicine. We have implemented SARA using the concatenation of orthonormal Daubechies wavelet bases and the Dirac basis. Experimental results demonstrate that the sparsity averaging prior embedded in SARA outperforms state-of-the-art priors that promote sparsity in a single orthonormal basis or redundant frame, or that promote gradient sparsity. In virtually all simulations, the sparsity averaging conjecture provided significantly better reconstruction qualities than any of the benchmark methods, both in terms of SNR and visual quality. These results appear even stronger when acknowledging the fact that the second best performance is not always given by the same method (RW-TV or RW-BPDb8), but depends on the simulated acquisition scheme and image of interest.

Note that dictionary learning/optimization has been proven very effective in CS (e.g. [27]) and highlights a future road for SARA. In particular, one may readily consider a rudimentary evolution of SARA where some of the frames used in the initial concatenation, but where the signal estimated by a first run of SARA (dictionary learning phase) is not sparse, might be removed for a second run of the algorithm (reconstruction phase). This suggests an algorithm where we estimate iteratively the signal and the best set of frames. Also in future work, we will study the possibility to move the orthonormal wavelet bases used in our implementation to translation invariant dictionaries using the cycle spinning method [46]. Future work should also study SARA in imaging inverse problems such as denoising, deblurring or inpainting.

APPENDIX A PROXIMITY OPERATORS

Let f be a convex lower semicontinuous function from \mathbb{R}^N to \mathbb{R} . The proximity operator of f is defined as:

$$\text{prox}_f(\mathbf{x}) \triangleq \arg \min_{\mathbf{z} \in \mathbb{R}^N} f(\mathbf{z}) + \frac{1}{2} \|\mathbf{x} - \mathbf{z}\|_2^2. \quad (13)$$

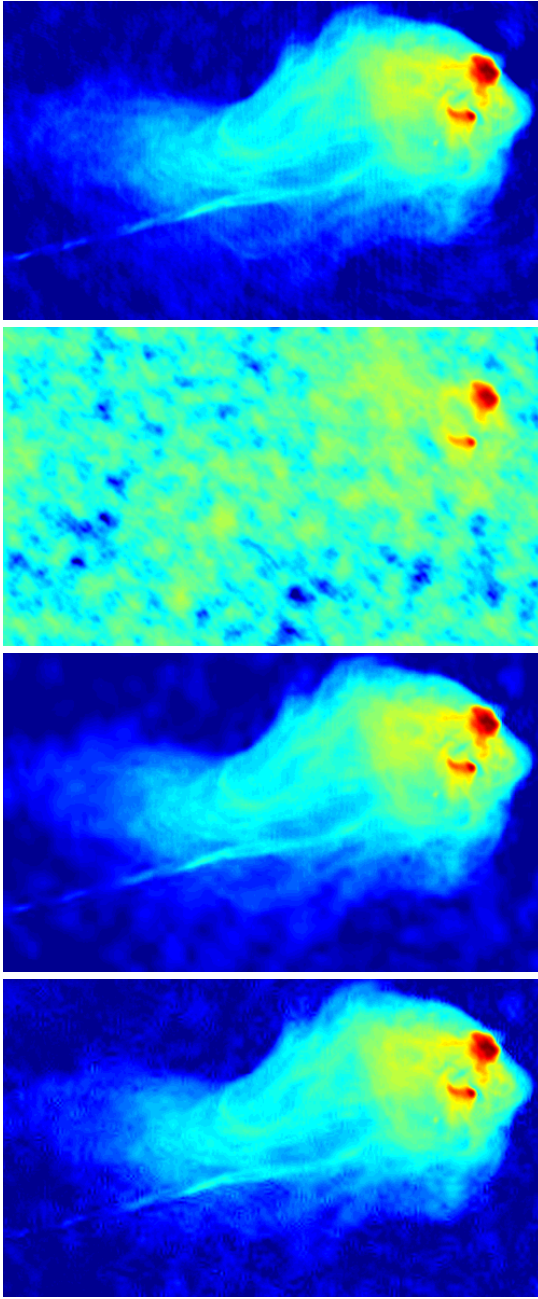


Figure 5. Astronomical image example, $M = 0.05N$ and ISNR set as 30 dB. From top to bottom: original image, backprojected image, reconstructed image by SARA (39.4 dB) and reconstructed image by RW-BPD8 (35.9 dB). All images are shown in a \log_{10} scale due to their high dynamic range.

Again complex-valued vectors are treated as real-valued vectors with twice the dimension. To compute the proximity operator of f_1 , let us first define the function

$$\ell(\boldsymbol{\alpha}) = \|\mathbf{W}\boldsymbol{\alpha}\|_1 = \sum_{i=1}^D \omega_i |\alpha_i|, \quad (14)$$

where $\omega_i = W_{ii}$ (since \mathbf{W} is a diagonal positive matrix). The function $\ell(\boldsymbol{\alpha})$ is the weighted ℓ_1 norm of $\boldsymbol{\alpha}$. The proximity operator of $\ell(\boldsymbol{\alpha})$ is given by $\text{prox}_\ell = \left\{ \text{prox}_{\omega_i|\cdot|}(\alpha_i) \right\}_{1 \leq i \leq D}$, where $\text{prox}_{\lambda|\cdot|}$ is the entry-wise soft-thresholding operator

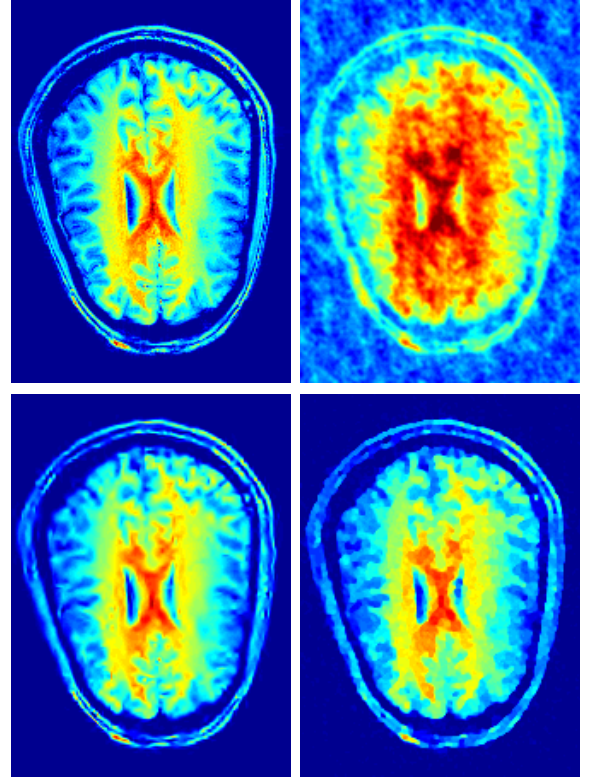


Figure 6. Brain image example. $M = 0.05N$ and ISNR set as 30 dB. First row: Original brain image (left) and the backprojected image (right). Second row: reconstruction results for SARA (left, 18.8 dB) and TV (right, 17.3 dB).

defined as

$$\text{prox}_{\lambda|\cdot|}(x) = \frac{x}{|x|} (|x| - \lambda)^+, \quad (15)$$

with $(\cdot)^+ = \max(0, \cdot)$. See [40] and references therein for a derivation of this result. The proximity operator of f_1 can be computed as follows. Let $0 < \mu_t < 2/\|\Psi^\dagger\|^2$, where $\|\cdot\|$ denotes the operator norm, and define the recursion

$$\begin{aligned} \mathbf{u}^{(t+1)} &= \mu_t \left(1 - \text{prox}_{\mu_t^{-1}\ell} \right) \left(\mu_t^{-1} \mathbf{u}^{(t)} + \Psi^\dagger \mathbf{v}^{(t)} \right) \\ \mathbf{v}^{(t+1)} &= \mathbf{x} - \Psi \mathbf{u}^{(t+1)}. \end{aligned} \quad (16)$$

Then $\mathbf{v}^{(t)} \rightarrow \text{prox}_{f_1}$ linearly [47]. The proximity operator of $f_2(\mathbf{x}) = i_{C'_\epsilon}(\mathbf{x})$ is the projector onto the convex set $C'_\epsilon = \{\mathbf{x} \in \mathbb{C}^N : \|\mathbf{y} - \Phi \mathbf{x}\|_2 \leq \epsilon\}$. If the reality and positivity constraint is active, computing the proximity operator of $f_2(\mathbf{x}) = i_{C'_\epsilon}(\mathbf{x})$, with $C'_\epsilon = C_\epsilon \cup \mathbb{R}_+^N$, is akin to solve a feasibility problem. We can decompose f_2 as

$$f_2(\mathbf{x}) = g(\Phi \mathbf{x} - \mathbf{y}) + h(\mathbf{x}), \quad (17)$$

where $h(\mathbf{z}) = i_{\mathbb{R}_+^N}(\mathbf{z})$, $g(\mathbf{z}) = i_{B_\epsilon}(\mathbf{z})$ and $B_\epsilon = \{\mathbf{z} \in \mathbb{C}^M : \|\mathbf{z}\|_2 \leq \epsilon\}$. Using this decomposition, we can use the dual forward-backward algorithm [40] to compute prox_{f_2} .

Let $0 < \kappa_t < 2/\|\Phi\|^2$ and define the recursion

$$\begin{aligned} \mathbf{p}^{(t+1)} &= \kappa_t \left(1 - \text{prox}_{\kappa_t^{-1}g} \right) \left(\kappa_t^{-1} \mathbf{p}^{(t)} + \Phi \mathbf{q}^{(t)} - \mathbf{y} \right) \\ \mathbf{q}^{(t+1)} &= \text{prox}_{\kappa_t^{-1}h} \left(\mathbf{x} - \Phi^\dagger \mathbf{p}^{(t+1)} \right), \end{aligned} \quad (18)$$

where $\text{prox}_h(\mathbf{z}) = \{(z_i)^+\}_{1 \leq i \leq N}$ and $\text{prox}_g(\mathbf{z}) =$

$\min(1, \epsilon/\|z\|_2)z$. Then $q^{(t)} \rightarrow \text{prox}_{f_2}$ linearly [40]. If the positivity constraint is not active, prox_h is replaced by the identity. In practice we accelerate the recursion in (18) using a Nesterov-type update [48].

REFERENCES

- [1] D. L. Donoho, "Compressed sensing," *IEEE Transactions on Information Theory*, vol. 52, no. 4, pp. 1289–1306, Sep. 2006.
- [2] E. J. Candès, "Compressive sampling," in *Proceedings, Int. Congress of Mathematics*, Madrid, Spain, Aug. 2006.
- [3] R. Baraniuk, "Compressive sensing," *IEEE Signal Processing Magazine*, vol. 24, no. 4, pp. 118–121, Jul. 2007.
- [4] M. Fornasier and H. Rauhut, *Handbook of Mathematical Methods in Imaging*. Springer, 2011, ch. Compressed sensing.
- [5] M. Duarte, M. Davenport, D. Takhar, J. Laska, T. Sun, K. Kelly, and R. Baraniuk, "Single-pixel imaging via compressed sensing," *IEEE Signal Processing Magazine*, vol. 25, no. 2, pp. 83–91, Mar. 2008.
- [6] R. Marcia, Z. Harmany, and R. Willett, "Compressive coded aperture imaging," in *Proceedings of SPIE Electronic Imaging: Computational Imaging VII*, San Jose, CA, 2009.
- [7] M. Lustig, D. L. Donoho, J. M. Santos, and J. M. Pauly, "Compressed sensing MRI," *IEEE Signal Processing Magazine*, vol. 25, no. 2, pp. 72–82, Mar. 2008.
- [8] G. Puy, J. Marques, R. Gruetter, J.-P. Thiran, D. V. De Ville, P. Vandergheynst, and Y. Wiaux, "Spread spectrum magnetic resonance imaging," *IEEE Transactions on Medical Imaging*, vol. 31, no. 3, pp. 586–598, Mar. 2012.
- [9] V. Studer, J. Bobin, M. Chahid, H. Moussavi, E. J. Candès, and M. Dahan, "Compressive fluorescence microscopy for biological and hyperspectral imaging," *Proceedings of the National Academy of Sciences USA*, vol. 109, no. 26, pp. E1679–E1687, 2012.
- [10] Y. Wiaux, L. Jacques, G. Puy, A. M. M. Scaife, and P. Vandergheynst, "Compressed sensing imaging techniques for radio interferometry," *Monthly Notices of the Royal Astronomical Society*, vol. 395, no. 3, pp. 1733–1742, 2009.
- [11] Y. Wiaux, G. Puy, Y. Boursier, and P. Vandergheynst, "Spread spectrum for imaging techniques in radio interferometry," *Monthly Notices of the Royal Astronomical Society*, vol. 400, no. 2, pp. 1029–1038, 2009.
- [12] R. E. Carrillo, J. D. McEwen, and Y. Wiaux, "Sparsity averaging reweighted analysis (SARA): a novel algorithm for radio-interferometric imaging," *Monthly Notices of the Royal Astronomical Society*, 2012, preprint, arXiv:1205.3123v3.
- [13] M. Figueiredo and R. Nowak, "An EM algorithm for wavelet-based image restoration," *IEEE Transactions on Image Processing*, vol. 12, no. 8, pp. 906–916, 2003.
- [14] M. Figueiredo, J. Bioucas-Dias, and R. Nowak, "Majorization-minimization algorithms for wavelet-based image restoration," *IEEE Transactions on Image Processing*, vol. 16, no. 12, pp. 2980–2991, 2007.
- [15] R. Gribonval and M. Nielsen, "Sparse representations in unions of bases," *IEEE Transactions on Information Theory*, vol. 49, no. 12, p. 33203325, Dec. 2003.
- [16] J.-L. Starck, M. Elad, and D. Donoho, "Redundant multiscale transforms and their application for morphological component analysis," *Advances in Imaging and Electron Physics*, vol. 132, 2004.
- [17] J. Bobin, J.-L. Starck, J. Fadili, Y. Moudden, and D. Donoho, "Morphological component analysis: an adaptive thresholding strategy," *IEEE Transactions on Image Processing*, vol. 16, no. 11, pp. 2675–2681, 2007.
- [18] J.-L. Starck, J. Fadili, and F. Murtagh, "The undecimated wavelet decomposition and its reconstruction," *IEEE Transactions on Signal Processing*, vol. 16, no. 2, pp. 297–309, 2007.
- [19] J. Starck, F. Murtagh, and J. Fadili, *Sparse Image and Signal Processing: Wavelets, Curvelets, Morphological Diversity*. Cambridge University Press, Cambridge, GB, 2010.
- [20] S. Lesage, R. Gribonval, F. Bimbot, and L. Benaroya, "Learning unions of orthonormal bases with thresholded singular value decomposition," in *Proc. IEEE Int. Conference on Acoustics, Speech and Signal Processing*, Philadelphia, PA, Mar. 2005.
- [21] R. Rubinstein, A. M. Bruckstein, and M. Elad, "Dictionaries for sparse representation modeling," *Proceedings of the IEEE*, vol. 98, no. 6, pp. 1045–1057, Apr. 2010.
- [22] H. Rauhut, K. Schnass, and P. Vandergheynst, "Compressed sensing and redundant dictionaries," *IEEE Transactions on Information Theory*, vol. 54, no. 5, pp. 2210–2219, May 2008.
- [23] E. J. Candès, Y. Eldar, D. Needell, and P. Randall, "Compressed sensing with coherent and redundant dictionaries," *Applied and Computational Harmonic Analysis*, vol. 31, no. 1, pp. 59–73, 2010.
- [24] E. J. Candès, "The restricted isometry property and its implications for compressed sensing," *Compte Rendus de l'Academie des Sciences, Paris, Series I*, vol. 346, pp. 589–593, 2008.
- [25] F. Krahmer and R. Ward, "New and improved johnson-lindenstrauss embeddings via the restricted isometry property," *SIAM J. Math. Anal.*, vol. 43, no. 3, pp. 1269–1281, 2011.
- [26] G. Puy, P. Vandergheynst, R. Gribonval, and Y. Wiaux, "Universal and efficient compressed sensing by spread spectrum and application to realistic fourier imaging techniques," *EURASIP Journal on Applied Signal Processing*, vol. 2012, no. 3, 2012.
- [27] G. Peyré, "Best basis compressed sensing," *IEEE Transactions on Signal Processing*, vol. 58, no. 5, pp. 2613–2622, May 2010.
- [28] E. J. Candès, M. Wakin, and S. Boyd, "Enhancing sparsity by reweighted ℓ_1 minimization," *Journal of Fourier Analysis and Applications*, vol. 14, no. 5, pp. 877–905, 2008.
- [29] D. Needell, "Noisy signal recovery via iterative reweighted ℓ_1 -minimization," in *Proceedings, Asilomar Conference on Signals, Systems and Computers*, Pacific Grove, CA, Nov. 2009.
- [30] E. J. Candès and J. Romberg, "Sparsity and incoherence in compressive sampling," *Inverse Problems*, vol. 23, no. 3, pp. 969–985, Apr. 2007.
- [31] J. A. Tropp and A. C. Gilbert, "Signal recovery from random measurements via orthogonal matching pursuit," *IEEE Transactions on Information Theory*, vol. 53, no. 12, pp. 4655–4666, Dec. 2007.
- [32] D. Needell and J. A. Tropp, "Cosamp: Iterative signal recovery from incomplete and inaccurate samples," *Applied Computational Harmonic Analysis*, vol. 26, no. 3, pp. 301–321, 2008.
- [33] T. Blumensath and M. Davies, "Iterative hard thresholding for compressed sensing," *Applied Computational Harmonic Analysis*, vol. 27, no. 3, pp. 265–274, 2009.
- [34] M. Elad, P. Milanfar, and R. Rubinstein, "Analysis versus synthesis in signal priors," *Inverse Problems*, vol. 23, no. 3, pp. 947–968, Jun. 2007.
- [35] S. Vaiter, G. Peyré, C. Dossal, and J. Fadili, "Robust sparse analysis regularization," 2011, preprint, arXiv:1109.6222v4.
- [36] A. Chambolle, "An algorithm for total variation minimization and applications," *Journal of Mathematical Imaging and Vision*, vol. 20, no. 1-2, pp. 89–97, 2004.
- [37] R. A. DeVore, B. Jawerth, and B. J. Lucier, "Image compression through wavelet transform coding," *IEEE Transactions on Information Theory*, vol. 38, no. 2, pp. 719–746, Jan. 1992.
- [38] J. Nocedal and S. Wright, *Numerical Optimization*. Springer, New York, 2006.
- [39] P. L. Combettes and J.-C. Pesquet, "A douglas-Rachford splitting approach to nonsmooth convex variational signal recovery," *IEEE Journal of Selected Topics in Signal Processing*, vol. 1, no. 4, pp. 564–574, Dec. 2007.
- [40] —, *Fixed-Point Algorithms for Inverse Problems in Science and Engineering*. Springer, New York, 2011, ch. Proximal splitting methods in signal processing, pp. 185–212.
- [41] A. R. Thompson, J. M. Moran, and G. W. Swenson, *Interferometry and Synthesis in Radio Astronomy*. Wiley-Interscience, New York, 2001.
- [42] Z. P. Liang and P. C. Lauterbur, *Principles of magnetic resonance imaging a signal processing perspective*. Wiley-IEEE Press, 1999.
- [43] G. Puy, P. Vandergheynst, and Y. Wiaux, "On variable density compressive sampling," *IEEE Signal Processing Letters*, vol. 18, no. 10, pp. 595–598, Oct. 2011.
- [44] F. Li, T. J. Cornwell, and F. de Hoog, "Application of compressive sampling to radio astronomy I: Deconvolution," *Astronomy & Astrophysics*, vol. A31, pp. 528–538, 2011.
- [45] C. L. Carilli and P. D. Barthel, "Cygnus A," *Astronomy & Astrophysics Reviews*, vol. 7, 1996.
- [46] R. Coifman and D. Donoho, "Translation invariant de-noising," in *Wavelets and Statistics, Lecture Notes in Statistics*, A. Antoniadis and G. Oppenheim, Eds. Springer, New York, 1995, vol. 103, pp. 125–150.
- [47] M. Fadili and J. Starck, "Monotone operator splitting for optimization problems in sparse recovery," in *Proc. IEEE International Conference on Image Processing*, El Cairo, Egypt, Nov. 2009.
- [48] A. Beck and M. Teboulle, "A fast iterative shrinkage-thresholding algorithm for linear inverse problems," *SIAM Journal on Imaging Sciences*, vol. 2, no. 1, pp. 183–202, 2009.